

Inverse photoemission

P. D. Johnson

Physics Department, Brookhaven National Laboratory, Upton, New York 11973

S. L. Hulbert

National Synchrotron Light Source, Brookhaven National Laboratory, Upton, New York 11973

(Received 25 October 1989; accepted for publication 11 May 1990)

We review the experimental apparatus presently available for use in inverse photoemission spectroscopy (IPES) in the vacuum ultraviolet (5–30 eV) energy range. We consider the design and use of different photon detectors including the gas-filled Geiger Muller counters and the more recent solid-state isochromat detectors. We review the properties of various tunable photon detectors employing either gratings or lenses as the dispersive element. Detection of the polarization of the photons and its role in the emission process is also discussed. A survey of the different electron gun designs is presented with a discussion of the limitations imposed by space-charge effects on both the available current and the achievable momentum resolution. Finally we present a brief review of spin-polarized IPES (SPIPES) and discuss the introduction of spin polarization in the incident electron beam.

I. INTRODUCTION

The last decade has seen the rapid development of inverse photoemission spectroscopy (IPES) as a technique for investigating the unoccupied states above the Fermi level in solids.¹ As such it complements the earlier technique photoemission spectroscopy (PES) which provides information on the occupied states.² In PES an incident photon excites an electron from an occupied state below the Fermi level to an unoccupied state above the Fermi level. Shown in Fig. 1 (a), the electron in this final state is the detected particle. Conversely, in IPES, Fig. 1 (b), an incident electron couples into an unoccupied state and makes a radiative transition to another unoccupied state above the Fermi level. The detected particle is now the photon emitted in the transition. Neglecting the required occupation of the initial state in PES, the two techniques are generally considered as time reversed processes.³ However, the two methods may be treated as time reversed only for delocalized systems as found in the solid state. For such systems it can be shown⁴ that the differential cross sections $d\sigma/d\omega$ for the two processes are related through the ratio R given by

$$R = \frac{(d\sigma/d\omega)_{IPES}}{(d\sigma/d\omega)_{PES}} = \left(\frac{\lambda_e}{\lambda_{h\nu}}\right)^2, \tag{1}$$

where λ_e and $\lambda_{h\nu}$ are the wavelengths of the emitted particles. This ratio is a reflection of the different densities of final states available for the two transitions. In the UV energy range R is approximately 10^{-5} and in the x-ray range approximately 10^{-3} . The low cross section for emission of photons in IPES is the principal reason for the relatively slow development of the technique as compared with PES. However, even with the problems associated with such a low cross section, IPES has advanced considerably, and indeed the analogs of many of the phenomena previously observed in PES have now also been observed in IPES spectra.

The unoccupied states above the Fermi level have been examined using a number of techniques other than IPES. These experimental methods include appearance potential

spectroscopy (APS)⁵ and near edge x-ray adsorption spectroscopy (NEXAFS)⁶ where, in both cases, core electrons are excited to unoccupied final states above the Fermi level. In the former case excitation is via incident electrons and in the latter case via photons. The unoccupied states have also been examined using two-photon spectroscopy.⁷ Here an initial photon excites an occupied state below the Fermi level to

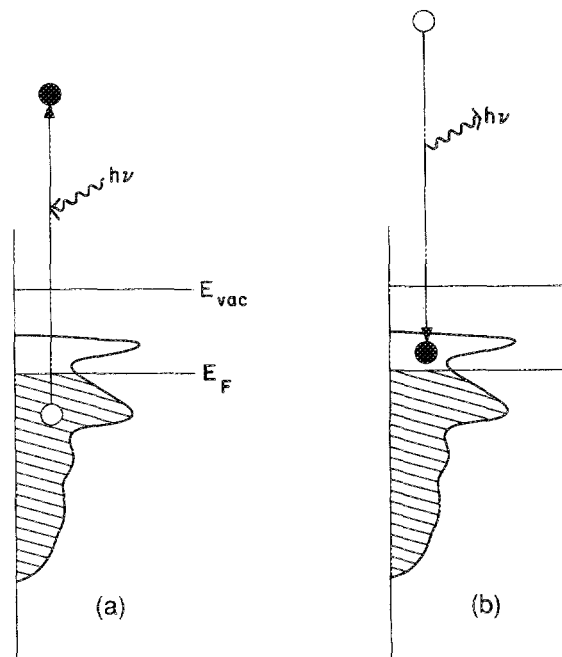


FIG. 1. Energy level diagram comparing photoemission (PES) with inverse photoemission (IPES). (a) In PES, a photon promotes an electron from a filled state below E_F to an unfilled state above E_{vac} . (b) In IPES, an electron that has coupled to an unfilled state above E_{vac} makes a transition to an unfilled state between E_F and E_{vac} with the emission of a photon.

an intermediate state above the Fermi level; this intermediate state is then probed by excitation with a second photon. The first two techniques, APS and NEXAFS, do not have the ability to map out the k dependence of the unoccupied states. IPES and two-photon spectroscopy share this ability. However, while the latter technique has demonstrated the highest energy resolution, it has not yet been possible to apply it to as wide a variety of experimental systems as IPES.

The basic experimental requirement of IPES is an electron source providing a well-defined beam and a photon detector with limited bandwidth. The sampling of the Brillouin zone in solid-state experiments is determined entirely by the angle of incidence of the electron beam. Having selected an angle of incidence, experiments are carried out either by scanning the incident electron beam energy and detecting photons emitted at a constant energy (isochromat mode) or by fixing the incident electron energy and collecting photons emitted over a range of energies (parallel detection, or spectrograph mode). In the isochromat mode, the parallel component of the crystal momentum k_{\parallel} is given by

$$k_{\parallel} = \left(\sqrt{\frac{2m_e}{\hbar^2}} \right) \sqrt{E_f + \hbar\omega - \phi} \sin \theta, \quad (2)$$

where m_e is the electron rest mass, E_f is the energy of the final state above the Fermi level, ϕ the work function of the material, $\hbar\omega$ the (fixed) photon energy, and θ the angle of incidence. In instruments capable of detecting photons at variable wavelengths, k_{\parallel} is given by

$$k_{\parallel} = \left(\sqrt{\frac{2m_e}{\hbar^2}} \right) (\sqrt{E_i - \phi}) \sin \theta, \quad (3)$$

where now E_i is the fixed incident electron energy defined with respect to the Fermi level. Example k -resolved inverse

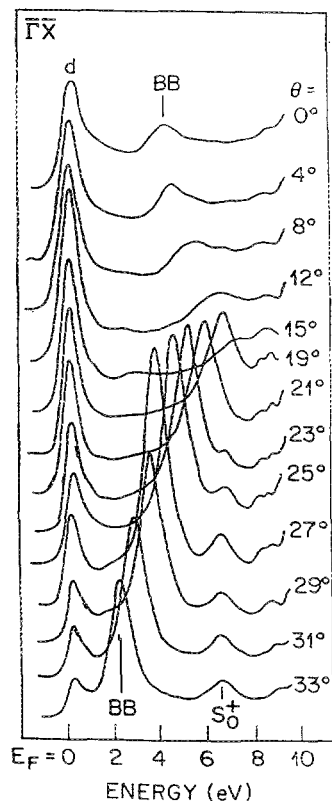


FIG. 2. KRIPES data taken on Pd(110) as a function of θ , the angle of electron incidence in the $\bar{\Gamma}\bar{X}$ azimuth. The incident electron energy was 22.5 eV relative to E_f . Features labeled BB are attributed to direct transitions within the bulk band structure. The feature labeled S_0^+ is identified as a surface state.

photoemission (KRIPES) spectra recorded from a Pd(110) surface as a function of the angle of incidence of the electron beam are shown in Fig. 2. The spectra were taken with fixed incident electron-beam energy and all emitted photons were detected in parallel using a spectrograph to be described later. Discussed in detail elsewhere,⁸ the spectra show dispersion of both bulk- (BB) and surface- (SS) derived bands.

In this article, we review the experimental problems associated with IPES. We examine the different photon detectors currently available and then discuss the various electron sources used in the technique. Our discussion will be limited to the generation of low-energy electrons and detection of photons in the UV range (5–30 eV). Photon emission in the x-ray range, or bremsstrahlung isochromat spectroscopy (BIS), has been reviewed elsewhere.⁹ The latter technique requires electron sources operating at higher kinetic energies (in the 1-keV range) and photon detection is generally accomplished with a crystal monochromator.

II. PHOTON DETECTORS

A. Isochromat detectors

The photon detectors used in IPES have fallen into two categories, those that operate in an isochromat or fixed photon energy mode and those that are tunable, allowing detection at different photon energies.

Detectors of the isochromat type include the Geiger Muller counter, which was introduced to the technique by Dose and co-workers.¹⁰ The construction of this detector, shown schematically in Fig. 3(a), is relatively simple: a stainless-steel tube, typically 25 mm in diameter, is closed at one end by a calcium fluoride (CaF_2) window and filled with iodine gas to a pressure determined by its room-temperature vapor pressure (0.1 Torr). The combination of the transmission properties of the window and the photoionization cross section of the gas determine the photon energy detected and the bandwidth, as shown in Fig. 3(b). A photon with an energy lower than the cutoff of the window but higher than the ionization potential of the gas will initiate an electron cascade which is collected by a central electrode. Samson¹¹ has noted that detectors of this type have the advantage of high sensitivity, low noise level, and complete insensitivity to wavelengths longer than the ionization potential of the gas. Several authors have reported improved stability with the introduction of helium at a partial pressure of approximately 400 Torr into the gas cell. The increase in pressure allows the detector to operate on the plateau region of its gain curve. As seen in Fig. 3(b), the standard combination of CaF_2 window and iodine vapor produces a photon detector centered at 9.7 eV with a band pass of approximately 0.8 eV.

A more recent development has been the replacement of the CaF_2 window by SrF_2 .¹² This moves the detected photon energy to 9.5 eV and reduces the bandwidth to 0.4 eV. The authors report a further reduction in the bandwidth if the temperature of the SrF_2 entrance window is raised from 20 to 70 °C. Any reduction in the bandwidth will of course be accompanied by a reduction in the transmission. Indeed, published spectra using a SrF_2 window¹² indicate that the

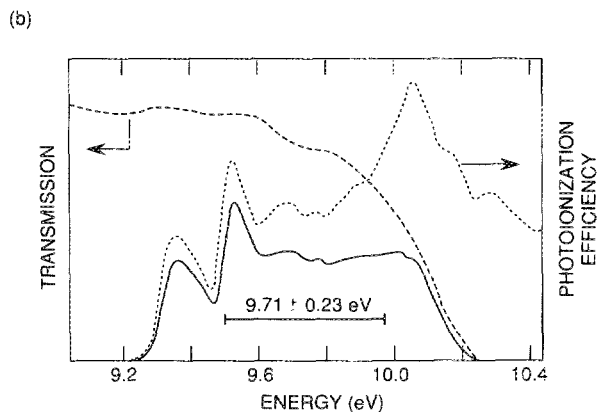
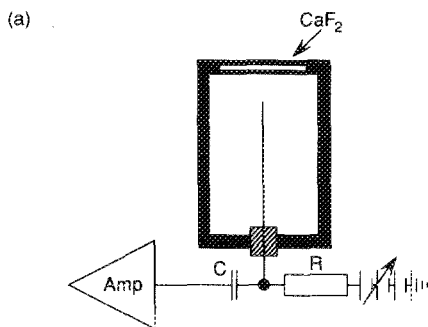


FIG. 3. (a) Schematic diagram of the Geiger Muller detector. The central electrode, floated to a positive potential, collects the electron cascade current generated by incident photons. (b) Bandpass characteristics of the Geiger Muller counter. Transmission of the CaF window (---), photoionization cross section of the iodine vapor (---), and the product of these two (—).

overall count rate decreases by approximately an order of magnitude compared to CaF₂.

A more complete description of the operation and construction of the Geiger Muller detectors is given by Samson,¹¹ who also details a number of other possible combinations of window and gas filling. Combinations that have already been used in IPES experiments include CaF₂/CS₂ detecting photons of energy 10.1 eV by Allen and co-workers¹³ and CaF₂/acetone by Funnemann and Merz.¹⁴ Geiger Muller counters have the advantage that they are capable of collecting photons from a large solid angle. As has been discussed elsewhere,³ the negligible momentum of the photon emitted in the IPES process makes it possible to collect a large solid angle of photons with no loss of resolution in crystal momentum space. The Geiger Muller detectors have therefore occasionally been combined with a mirror to increase the solid angle of collection, a geometry shown in Fig. 4.¹⁵ The reflectivity of such mirrors in the UV range may be improved by coating with Os or MgF₂. At normal incidence, the reflectance of a 250-Å-thick MgF₂ film at a wavelength of 1200 Å is, for example, approximately 70%.¹⁶

As an alternative to the use of a photoionization

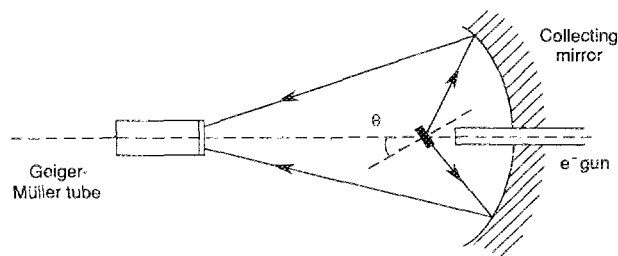


FIG. 4. Typical fixed wavelength IPES configuration, consisting of a Geiger Muller counter combined with a large collection mirror.

chamber, Babbe *et al.*¹⁷ have described a bandpass detector with bandwidth determined by the transmission properties of a CaF₂ window and the photoemission threshold of the first dynode of an electron multiplier. By evaporating a thin film of KBr onto the dynode, which operates as the high-pass photocathode, this group were able to increase the efficiency by a factor of 3.5.¹⁸ The authors report that this simple arrangement produces a photon detector with maximum efficiency at an energy of 9.8 eV and bandwidth 0.6 eV, comparable with the original Geiger Muller counters. However, by using a "solid state" detector or electron multiplier, the problems associated with the corrosive iodine vapor are avoided.

B. Tunable detectors

The second class of photon detectors employed in IPES relies on optical elements giving energy dispersion of the emitted photons. We describe two instruments falling within this class: first, the grating spectrograph, where the dispersive element is a ruled grating, and second, the so-called "lens refractor," where the dispersive element is a lens. Some of the basic experimental arrangements using these two detectors are shown schematically in Fig. 5.

The first spectrometer designed specifically for IPES experiments was based on a holographically ruled toroidal grating.¹⁹ In the original design, this instrument was capable of detecting photons in the range from 10–100 eV but was limited by the use of single-channel detection. Because of the relatively large (i.e., near grazing) angle of incidence of the photons on the grating, this type of spectrometer collects only a small solid angle of the radiation emitted from the sample. For the original instrument, the solid angle collected was 3×10^{-3} Sr (19° grazing angle of incidence on a 3 cm × 3 cm grating), resulting in a published photon detection rate of 300 counts eV⁻¹ s⁻¹ for a 1-mA electron-beam current on the sample. The instrument had 32-cm entrance and exit arm lengths and a 550 line/mm grating, producing a resolution that was typically 0.25 eV at 20 eV and 0.85 eV at 40 eV. More recently, this design, shown in Fig. 5(a), has been improved through the introduction of multichannel detection of the different wavelength photons.²⁰ The use of multichannel detection, described in more detail in Sec. II C

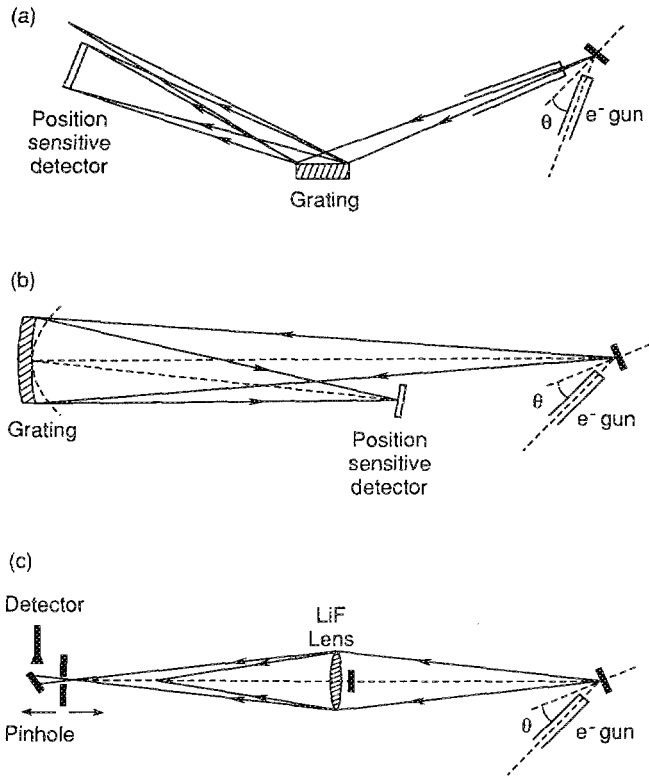


FIG. 5. Variable photon wavelength detectors used in IPES. (a) Grazing incidence spectrograph with toroidal grating and parallel detection. (b) Off-Rowland circle normal incidence spectrograph with parallel detection. (c) Refractor with a lens as the dispersing element and single channel detection.

below, is common to most spectrographs currently used in IPES.

Subsequent grating spectrographs have been of the normal incidence type and have used spherical gratings. The use of normal incidence restricts detection to photons of energy typically less than 40 eV. Elsewhere we have presented the principles governing the optical design of such instruments.²¹ The wavelength of detection in any spectrograph is given by the grating equation

$$\sin \alpha + \sin \beta = m\lambda / d, \quad (4)$$

where α and β are the angles of incidence and exit, respectively, m the order of diffraction, and d the line spacing. The optical path function F for a concave grating with equal groove spacing d , illuminated by a point source in the median (x - y) plane, is given by the following power series expansion in the tangential (y) and sagittal (z) spatial coordinates (see Fig. 6):

$$F = r + r' + [\sin \alpha + \sin \beta - (m\lambda / d)]y + C_{20}y^2 + C_{02}z^2 + \text{higher order terms.} \quad (5)$$

Here r and r' are the entrance and exit arm lengths and the C 's are terms relating to defocus (C_{20}) and astigmatism (C_{02}) in the exit plane. The condition for the source to be brought to a stigmatic focus is given by the minimization of F with respect to the y and z coordinates:

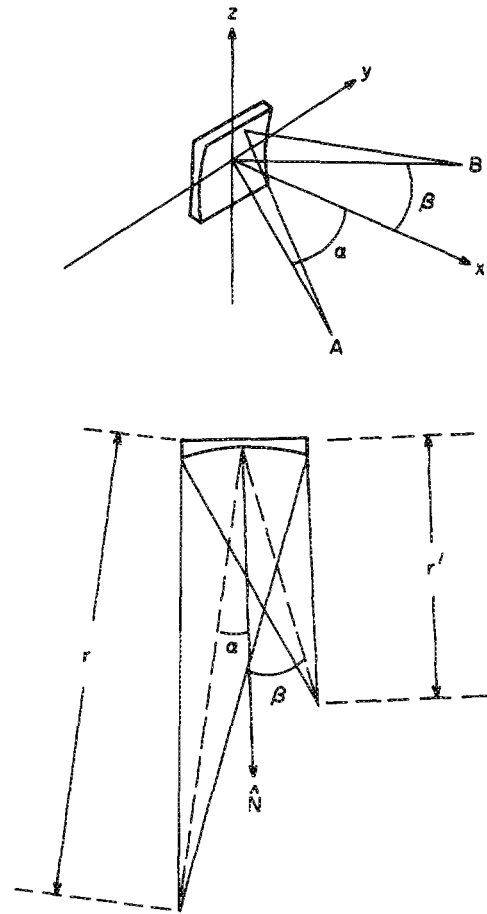


FIG. 6. Schematic diagrams of the spherical grating configuration showing (a) the coordinate system, and (b) the parameters involved in the equations describing the optical system.

$$\frac{\partial F}{\partial y} = 0, \quad \frac{\partial F}{\partial z} = 0. \quad (6)$$

This requires that $C_{20} = C_{02} = 0$. However, since all of the normal incidence spectrograph detectors described in this paper integrate in the sagittal (z) direction, pure astigmatism (C_{02}) does not affect their performance. Minimization of the defocus (C_{20}) terms lead to

$$T + T' = 0, \quad (7)$$

where

$$T = \left(\frac{\cos^2 \alpha}{r} - \frac{\cos \alpha}{R} \right)$$

and

$$T' = \left(\frac{\cos^2 \beta}{r'} - \frac{\cos^2 \beta}{R} \right),$$

and R is the radius of the grating.

If T and T' in Eq. (7) are separately set equal to zero we have the Rowland circle condition, giving

$$r = R \cos \alpha \quad \text{and} \quad r' = R \cos \beta. \quad (8)$$

Thus, for this configuration, the object and image points lie

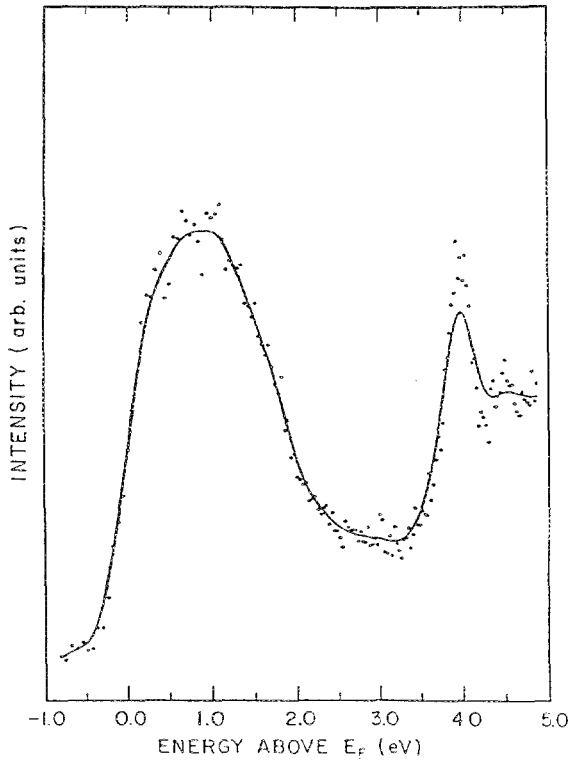


FIG. 7. Inverse photoemission spectrum from a Cu (001) surface showing the image state approximately 4.0 eV above the Fermi level. The electron beam is incident along the surface normal at an energy of 16.85 eV above the Fermi level. The dots represent the raw data and the solid line a smoothed fit.

on a circle of diameter R centered on the pole of the grating. Two instruments based on this solution have been successfully built by Himpfel and co-workers.^{22,23} The most recent design uses a spherical holographic grating with a radius of 750 mm and a line density of 1000 lines/mm. The acceptance of the grating is $f/3.5$ (i.e., the tangential aperture $\sim R/3.5$). With such an arrangement and an electron source to be described later, an energy resolution of approximately 300 meV at an energy of 15.5 eV has been achieved.

An alternative design based on the spherical grating has been described in our earlier paper.²¹ Rather than using the Rowland circle configuration, it is possible to find an acceptable solution with the entrance slit displaced further from the grating and, hence, the image closer [see Fig. 5(b)]. Using a nearly identical grating to that in the Rowland circle instrument²³ described above, it was found that an acceptable solution for the off-Rowland circle configuration²¹ placed the source at 975 mm with the image at approximately 610 mm. These values correspond to a small-angle ($\cos \alpha \approx \cos \beta \approx 1$) approximate solution to Eq. (7) with

$$r = \frac{13}{10}R \text{ and } r' = \frac{13}{16}R, \text{ so that } \frac{r'}{r} = \frac{5}{8}. \quad (9)$$

Such an arrangement allows the photon sensitive detector to be placed outside of the main experimental chamber with a consequent reduction in the required shielding.

The most significant third-order term in the expansion of the optical path function F , given in Eq. (5), is coma (C_{30}), the minimization of which requires that

$$\frac{\sin \alpha}{r}T + \frac{\sin \beta}{r'}T' = 0. \quad (10)$$

For the Rowland circle instrument, coma vanishes because T and T' vanish separately. In an off-Rowland circle instrument, however, coma may not be negligible if the tangential acceptance of the grating is too large (i.e., if the f number is too small). The resolution degradation due to coma varies as the square of the grating aperture in the tangential direction, or inversely as the square of the f number. For the typical operating condition of the off-Rowland circle instrument described here and in our earlier paper²¹ ($f/3.75$ aperture, source size ≈ 1 mm, image size ≈ 0.6 mm, $h\nu = 15$ eV) the energy spread due to coma is only $\frac{1}{3}$ of that due to the finite source size. Added in quadrature, this coma contribution is thus only 10% of the total energy spread. Opening the aperture by a factor of 2 (i.e., doubling the tangential dimension of the grating) would lead to the energy resolution of the instrument being dominated by coma, its contribution becoming $\frac{1}{3}$ of that due to the finite source size.

The off-Rowland circle instrument has achieved an energy resolution identical to that for the Rowland circle device²³ with essentially no loss in collection efficiency ($f/3.75$ vs $f/3.5$). Indeed, at low energies an overall energy resolution of approximately 300 meV is typically obtained as determined by the FWHM of the first member of the Rydberg series of image states, Fig. 7. These states are formed when an electron becomes trapped in the one-dimensional potential well formed between the long-range image potential on one side and a crystal band gap on the other.²⁴ Elsewhere, it has been shown that because of their location outside of the surface, the negligible lifetime broadening of such states will mean that their width is effectively determined solely by the instrumental resolution.²⁵ They thus provide an excellent test of the capabilities of any instrument. An energy resolution of approximately 300 meV represents the overall resolution of the system, electron source plus photon detector. A measure of the resolution of the photon detector independent of the energy spread of the electron source is obtained from the observed width of fluorescence lines.

Both of the normal incidence spectrographs described above have reported the observation of Lyman- α radiation emitted from excited hydrogen atoms leaving the surface. A typical spectrum is shown in Fig. 8. An incoming electron raises the hydrogen atom to an excited state which then reradiates after the atom has left the surface.²⁶ The width of the emitted line will therefore be independent of the energy spread in the incident electron beam. The Rowland circle instrument has reported a linewidth for the Lyman- α line of 18 Å or 160 meV for an effective entrance slit width of 1.2 mm.²³ For the same line the authors of the off-Rowland circle instrument have reported a FWHM of 0.1 eV for an effective 1-mm slit.²⁰ It should be noted that whereas the shape of the focal surface at the image distance is not flat (for either the Rowland circle or off-Rowland circle devices), the error introduced by using planar multichannel-plate detectors is

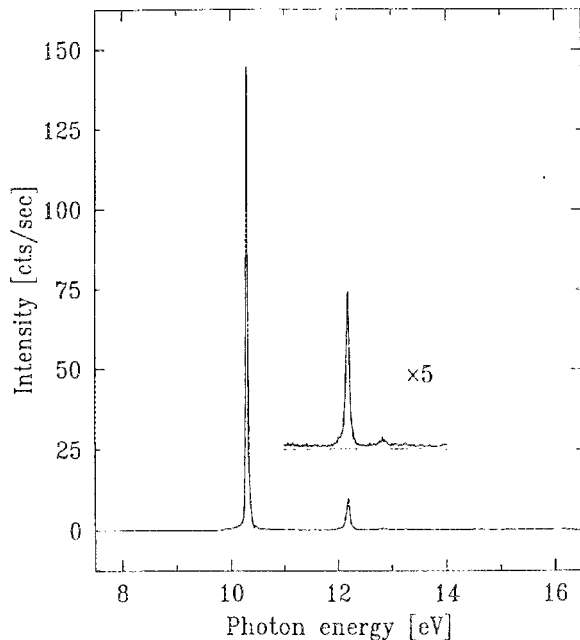


FIG. 8. Lyman- α (10.2 eV) and - β (12.1 eV) emission from $5L$ of hydrogen adsorbed on potassium-covered Ni(001) at room temperature. The incident electron beam energy is 30 eV with respect to the Fermi level E_F .

very small (the detector subtends typically only 40–80 mrad at the grating).

In all of the spectrographs, the photon detector is sensitive to the impact of electrons, ions, and stray UV photons in addition to the desired signal. Charged particle problems can be removed with appropriate electrostatic shielding of the detector, and stray light has to be minimized. These shielding requirements give the off-Rowland circle design the advantage that all of its components can be installed in a separate chamber from the electron source and sample.

A second type of tunable photon detector, employing a dispersive optical element, is the so-called “lens refractor,” in which the diffraction of the grating in the spectrometers is replaced by the refraction of a lens [Fig. 5(c)]. In particular, this instrument recognizes that near the appropriate cut-off energy, a lens manufactured from an alkali halide shows a strong wavelength dependence in its focal properties. Thus, detection at different wavelengths is achieved simply by moving an exit aperture along the dispersion axis. Laporte and Subtil²⁷ found that the refractive index, n , of LiF as a function of photon energy can be represented by the formula:

$$n^2 = 1 + \frac{34.76(E_0^2 - E^2)}{(E_0^2 - E^2)^2 + \gamma^2 E^2} + \frac{236.6}{E_1^2 - E^2} \quad (11)$$

where $E_0 = 12.632$ eV, $E_1 = 18.37$ eV, and $\gamma = 0.33$ eV. Using ray tracing, Childs, Royer, and Smith^{28,32} demonstrated that a symmetrical biconvex singlet LiF lens with source to lens distance $u_0 = 2f_0 = 500$ mm selects 9.1 eV photons with the pinhole distanced 850 mm from the lens and 11.08 eV photons with the pinhole at 350 mm. f_0 is the focal length at

$E = 10.2$ eV. Using a 2-mm aperture, the respective bandwidths at these different energies were approximately 0.4 and 0.15 eV. A practical demonstration of the capabilities of this instrument was provided by Hulbert *et al.*²⁹ While the tunability of a given lens is limited to a narrow photon energy range (typical 2–3 eV), the use of different alkali halides for the lens allows the refractor to be a useful instrument over a slightly larger range. We would emphasize that while tunable, the “refractor” is essentially an isochromat detector in that, having selected a wavelength of interest, the energy of the incident electron beam is scanned.

C. Photon sensitive surfaces

In this section we examine the various photon sensitive surfaces employed in these instruments. It is well documented in the literature that evaporation of a thin film of an alkali halide on a metal surface will increase the efficiency of photon detection in the UV range by a factor of from 3 to 4.¹¹ The multichannel plates used in the spectrograph designs have been coated with CsI or CuI, either evaporated *in situ* or “as bought” commercially. These surfaces tend to degrade as a function of time when exposed to the atmosphere, but it would appear from our own experience that the standard techniques used for achieving UHV conditions (i.e., baking to 100–150 °C under vacuum) will restore their properties. As already noted, thin films of KBr have also been used to improve the efficiency of detection in the “solid state” isochromat detectors.¹⁷

When using a photon sensitive surface in a tunable photon detector, it is necessary to calibrate the efficiency of the instrument as a function of photon wavelength. Ideally, this would be accomplished by using a well-defined or calibrated photon source. In practice, for the spectrographs that have been constructed to date, the relative efficiency as a function of wavelength has been measured by irradiating the photon sensitive surface with the bremsstrahlung radiation emitted when the target or sample is hit by a high-energy electron beam.

The use of multichannel detection in the spectrographs serves to compensate for the small solid angle of collection. The multichannel detector, Fig. 9, typically consists of a chevron (two channel plates stacked together) backed by a resistive sheet or encoder. The photon strikes the front surface of the chevron and initiates an electron cascade which is collected on the encoder. For a one-dimensional detector, the position of the photon is determined by the ratio $A/(A+B)$ of the measured charge pulses, A and B , reaching the two ends of the encoder. However, it is necessary to measure and compensate for the linearity of the encoder as a function of position. This may be achieved either by stepping a specularly reflected beam from the grating across the front surface of the detector or, for a fixed grating setting, by stepping the position of a well-defined feature such as the Fermi edge across the surface.

A typical electronic arrangement for measuring the position is also shown in Fig. 9. Charge pulses from the ends of the encoder are fed via charge-sensitive preamplifiers to linear gate and stretcher amplifiers. The latter amplifiers serve to remove any ambiguity that might be introduced in determining the peak position of the respective pulses. The

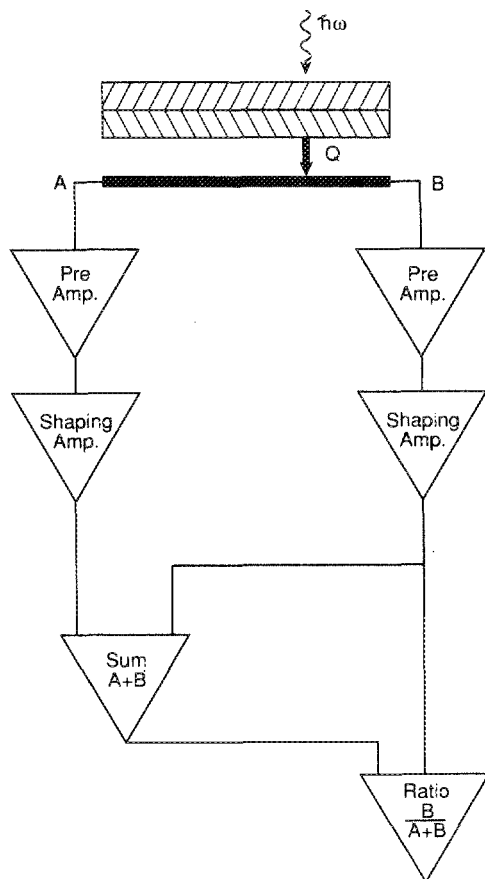


FIG. 9. Schematic diagram showing chevron microchannel-plate (MCP) photon detector and associated electronics.

stretched pulses are directed through summing and ratio circuits to provide the ratio $A/(A+B)$ which is then directed to a pulse height analyzer. The collected spectrum is normalized for linearity and wavelength efficiency.

It should be noted that the design of the off-Rowland circle spectrograph described earlier differs from the other instruments in that rather than operating with a fixed entrance slit it relies on the focused beam of the electron source. It is therefore necessary to have the flexibility of being able to position the sample at the appropriate source point to maintain the energy calibration of the detector. The easiest solution to this problem is to design the instrument such that it is possible to monitor the position of the zero order, or specularly reflected, beam from the grating.

As a guide for comparison, we show in Table I the energy, energy resolution, collection solid angle, detection efficiency (counts/collected photon), and transmission (counts/emitted photon) of the various photon detectors used for IPES. The transmission is evaluated as the product of the collection solid angle and the detection efficiency; the overall count rate can be approximated as the product of the transmission and the fractional bandwidth of the detector.

D. Polarization

As yet there has been little attention applied to measuring the polarization of the photons emitted in the IPES process. As in the analogous PES experiment, the initial and final states are coupled through the operator $A \cdot p$. Thus, knowing the polarization of the light, selection rules may be invoked to determine allowed transitions. In PES, where the final state has even symmetry, such rules have frequently been applied to determine the symmetry of the initial state both for solid-state transitions and for adsorbed atoms and molecules.² Obviously, the more linearly polarized the incident radiation, the easier it becomes to apply these symmetry arguments. Indeed, synchrotron radiation based experiments have seen their most extensive application.

The photon detectors that are currently used in IPES, particularly the Geiger Muller counters and the normal incidence spectrographs, show no selective sensitivity to the polarization of the photons. Consequently, all discussion of polarization effects has been influenced by the relative orientation of the sample and the detector. With the sample normal facing towards the detector the detected photon is effectively *s* polarized at the surface whereas with the sample normal perpendicular to the detector axis the detected photon has a greater component of *p* polarization. If the detector position is fixed, these two different configurations have generally been achieved by rotating the sample either towards or away from the detector. However, this has the result that another variable, the angle of incidence of the electron beam, has also been altered in the process of measurement. In order to circumvent this latter problem, different experimenters have used one of two solutions.

One solution is to use more than one detector in the same experiment, i.e., one that is positioned to favor *p*-polarized photons and a second that favors *s*-polarized photons. Here again *p* and *s* refer to the effective polarization at the surface. Figure 10 shows spectra obtained using an instrument of this type.³⁰ The spectra were recorded from a Ni(111) surface following exposure to 3L of oxygen and taken at two different photon collection angles. The difference between the two spectra clearly shows that the absorbate-induced feature at 1.35 eV above the Fermi level has A_1 symmetry, i.e., p_z derived. The spectra show that the image state located 5.5 eV above the Fermi level also has this symmetry.

An alternative solution has been to allow both the sample and the electron source to move.^{31,32} In designs of this type, the relative orientation of the source and sample may be fixed but the relative orientation of detector and sample varied. It may be anticipated that future designs will pay more attention to the effects of polarization.

III. ELECTRON SOURCES

In this section we review the development of electron sources used in IPES experiments. As the technique has progressed the electron source or gun clearly has become the critical item determining the ability to perform *k*-resolved measurements with reasonable angular or momentum resolution. Further, with the improvement in energy resolution

TABLE I. Energy, energy resolution, collection solid angle, detection efficiency (counts/collected photon), and transmission (counts/emitted photon) of the various types of photon detectors used for IPES.

	Isochromat Detectors			Spectrometers/Spectrographs		
	Geiger Muller: CaF ₂ /I ₂	Geiger Muller: SrF ₂ /I ₂	Electron multiplier: CaF ₂ /KBr	Grazing incidence: TGM	Normal incidence: NIM	Lens refractor
$h\nu$ (eV)	9.7	9.5	9.8	10-100	5-40	9-11
$\Delta(h\nu)$ (eV)	0.8	0.4	0.6	0.25@20 eV 0.85@40 eV	0.1@10 eV 0.4@20 eV	0.4@9.1 eV 0.15@11 eV
Collection solid angle (sr)	0.27 π^a	0.27 π	0.27 π	0.001 π	0.0095 π^b	0.015 π^c
w/collecting mirror ^d	0.71 π	0.71 π	0.71 π			
Approx. relative detection efficiency (counts/collected photon)	0.12 ^e	0.04 ^f	0.045 ^g	0.03 ^h	0.045 ⁱ	0.038 ^j
Approx. relative transmission (counts/emitted photon)						
w/collecting mirror	1.0 $\times 10^{-1}$ 2.7 $\times 10^{-1}$	3.4 $\times 10^{-2}$ 8.9 $\times 10^{-2}$	3.8 $\times 10^{-2}$ 1.0 $\times 10^{-1}$	9.4 $\times 10^{-5}$	1.3 $\times 10^{-3}$	1.8 $\times 10^{-3}$

^a 1 in. diam @ 1 in.

^b 150 mm \times 200 mm @ 1 m.

^c 4 in. diam @ 16 in.

^d 40° < θ < 90°, 0 < ϕ < 2 π .

^e CaF₂ transmission 30%, I₂ photoionization efficiency 40%.

^f SrF₂ transmission 10%, I₂ photoionization efficiency 40%.

^g CaF₂ transmission 30%, KBr/multiplier efficiency 15%.

^h Grazing incidence grating first order diffraction efficiency 20%, CsI/microchannel-plate efficiency 15%.

ⁱ Normal incidence grating first order diffraction efficiency 30%, CsI/microchannel-plate efficiency 15%.

^j LiF transmission 25%, CsI/microchannel plate efficiency 15%.

of the photon detectors, as detailed in the previous section, the energy spread of the electron source can be the key component in determining the overall energy resolution of the apparatus.

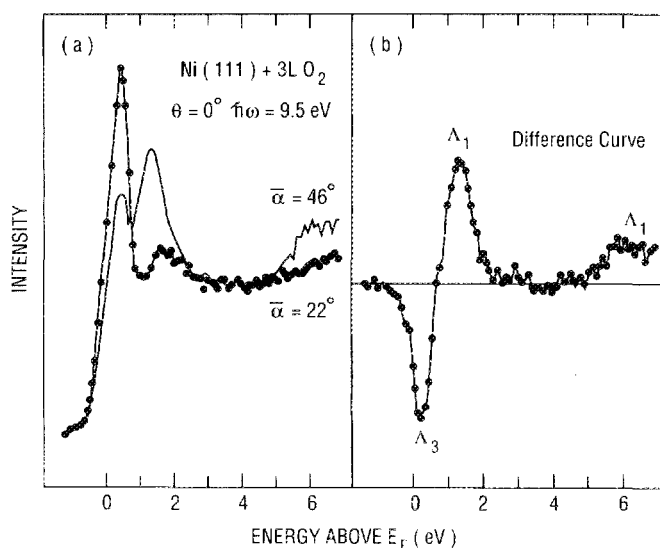


FIG. 10. (a) Inverse photoemission spectra from a Ni(111) surface following exposure to 3L of oxygen (Ref. 30). The spectra were recorded with a normally incident electron beam and at two different photon collection angles $\bar{\alpha}$. (b) The difference curve between the two spectra in (a), highlighting the symmetries of different peaks.

Early IPES studies with an apparatus that simply consisted of the Geiger Muller photon detector and a hot tungsten filament as the electron source, demonstrated that density of states information could be obtained.³³ The introduction to IPES of an electron source with a well-defined momentum spread gave clear evidence for direct k -conserving transitions of the type previously observed in PES.³⁴

The typical requirements of electron sources for IPES have been discussed in detail by Stoffel and Johnson.³⁵ The ideal source would provide a large current at low energies into a well-focused image with narrow angular spread in the beam. However, the ability to achieve the conflicting requirements of high currents and low energies is restricted by fundamental limits imposed by space-charge effects. In any design it is to be recognized that the space-charge-limited current density at a cathode varies as the three-halves power of the extraction voltage and inversely as the square of the cathode-anode distance. For a focused electron beam, the maximum current I_{\max} that can be directed onto a surface is given by

$$I_{\max} (\mu\text{a}) = 38.5 \tan^2(\theta_m/2) V^{3/2} (\text{volts}), \quad (12)$$

where eV is the energy of the incident beam referenced to the vacuum level and θ_m is the included angle.³⁶ The limitations imposed on I_{\max} by Eq. (12) are shown graphically in Fig. 11, where contours of I_{\max} are plotted as a function of the included angle and beam kinetic energy E_k . If a cathode is placed near the sample surface and a voltage V_c is applied

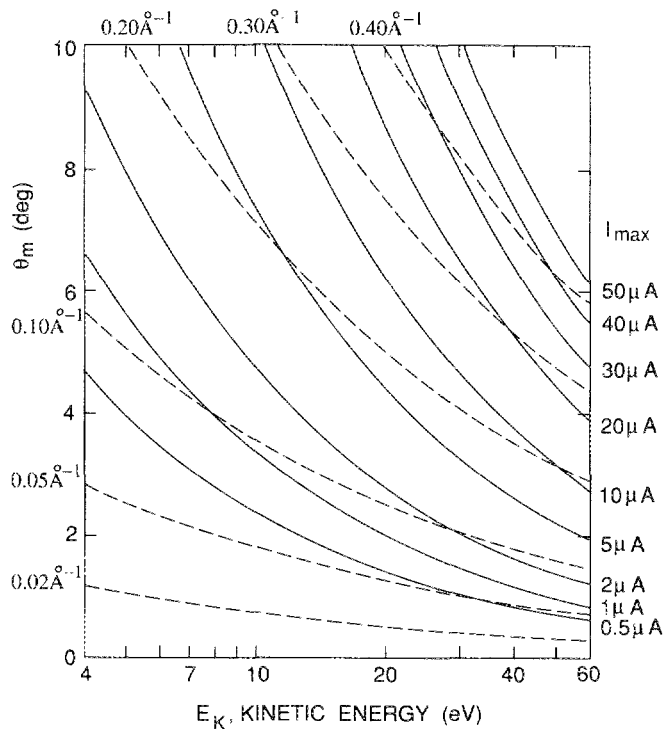


FIG. 11. Electron gun included angle in degrees vs kinetic energy with respect to the vacuum level. Solid lines show the space-charge-limited currents as defined by Eq. (12). Dashed lines indicate the parallel momentum resolution as defined in Eq. (14).

between them, the energy of the electrons with respect to the sample Fermi level is given by

$$E_i = eV_c + \phi_c, \quad (13)$$

where Φ_c is the work function of the cathode. E_k , or eV , the energy with respect to the vacuum level, is simply E_i minus the work function of the sample.

The ability to map dispersing bands, as shown earlier in Fig. 2, is limited by the momentum resolution of the incident electron beam. We show in Fig. 11 contours of constant momentum resolution Δk_{\parallel} for normal incidence as defined by the derivative of Eq. (3):

$$\Delta k_{\parallel} = \left(\sqrt{\frac{2m_c E_k}{\hbar^2}} \right) \cos \theta \Delta \theta. \quad (14)$$

Examination of Fig. 11 and Eqs. (12) and (14) shows that as the incident beam energy is increased, the space-charge-limited current increases but the momentum resolution decreases if the included angle is not reduced.

Within the limitations imposed by space-charge effects, Stoffel and Johnson³⁵ have discussed the design of an electron source whereby electrons are extracted from a cathode at high energy and subsequently decelerated and refocused onto the sample. Using a diode extraction source and a three-element refocusing lens [see Fig. 12(a)], they have been able to produce electrons with kinetic energies ranging from 5 to 40 eV. At the higher kinetic energies in this range, electron currents typically greater than 10 μA are produced in a

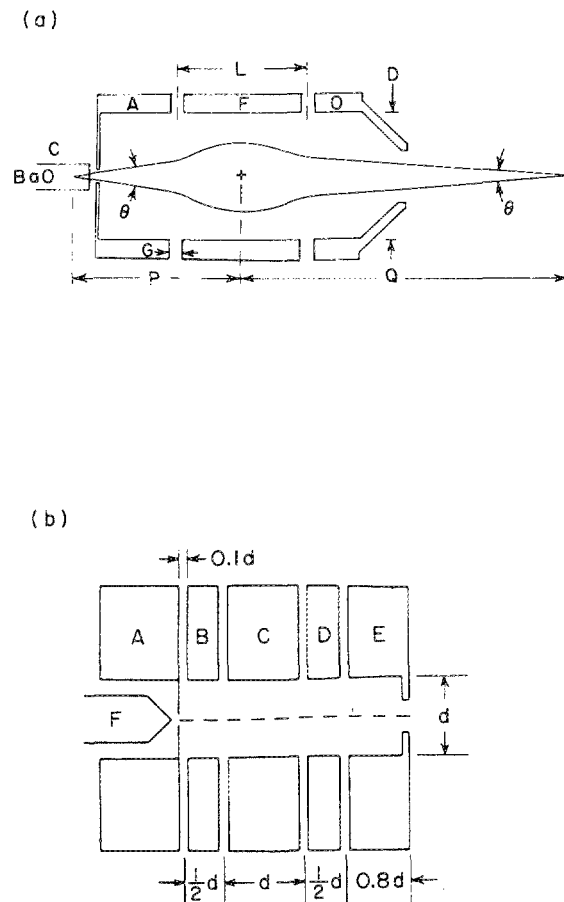


FIG. 12. (a) Schematic diagram of the Stoffel-Johnson electron gun design. C and A represent the diode extraction source. A, F, and O (ground potential) represent the three element lens. $L = D = 16 \text{ mm}$, $Q = 2.5 D$ and $P = 1.3 D$. (b) Schematic diagram of the Erdman-Zipf source. F, A, and B represent the triode extraction source. B, C, and D represent the three element lens and E, the output optic, is set at ground potential.

beam focused into a spot 1 mm in diameter. The source operates down to energies as low as 5 eV and has a full angular width of the order of 5° to 7° , a convergence corresponding to a momentum broadening of the order of 0.1 \AA^{-1} at 5 eV and 0.2 \AA^{-1} at 20 eV. The energy resolution of the electron beam is determined by the temperature of the BaO cathode and is typically 270 meV. We note that the alternative use of osmium-coated BaO cathodes can lower this energy spread to 220 meV.

Several other authors³⁷ have chosen to follow a design of Erdman and Zipf.³⁸ Their compact gun, shown in Fig. 12(b), consists of a filament spaced closely to a grid which contains a small aperture. This element is followed by a three element lens operated in the einzel mode; a final element serves to decelerate the electrons to produce a collimated beam. The filament, grid, and first element of the einzel lens represent the elements of a triode extraction source. Erdman and Zipf have established operating conditions that produce high beam currents down to low voltages. However, they did not measure the angular divergence of the beam and further,

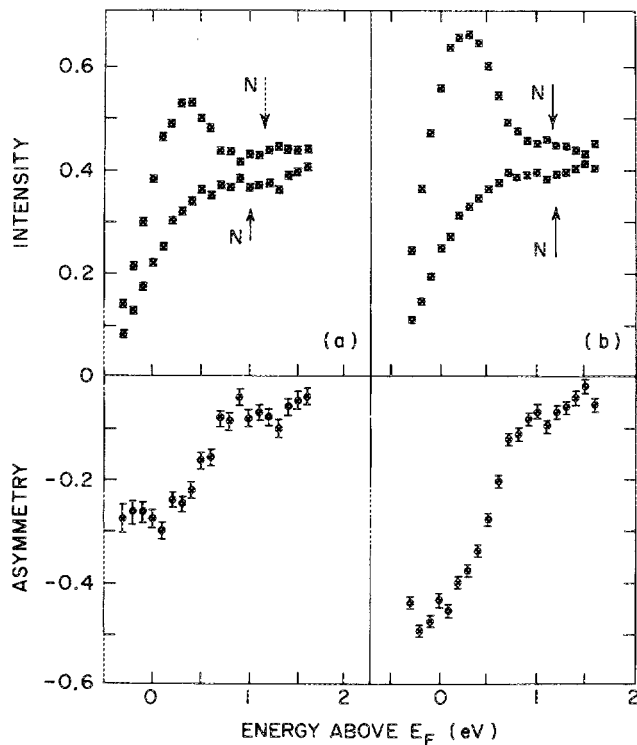


FIG. 13. SPIPES spectra recorded from a Ni(110) surface for (a) angle of incidence $\alpha = 0^\circ$, and (b) angle of incidence $\alpha = 20^\circ$. The spectra show the spin-resolved intensities $N\uparrow$ and $N\downarrow$, and the asymmetry A .

they assumed a diameter of 1 mm for the beam based on luminosity from the excitation of the background gasses in their vacuum chamber. Virtually all experimenters that have subsequently used this design for IPES experiments have replaced the tungsten filament by a BaO cathode. The most extensive published investigation of this latter type of source in an IPES application has been that by Brenac.³⁹

In comparing the simpler design due to Stoffel and Johnson with that due to Erdman and Zipf we would conclude that the former design is probably the better source for lower kinetic energies (< 30 eV) whereas the latter is better at higher energies. Brenac³⁹ has observed that at the higher energies the diode extraction source suffers losses due to large angular divergences from cathode to anode. This problem is reduced by the introduction of the triode source.

As an alternative to the use of an electron gun we note that the requirement of an intense electron beam led Fauster *et al.*²² to the use of the more simple Pierce diode gun in their instrument. The Pierce arrangement is essentially a diode source without a refocusing lens and with the sample replacing the extraction anode. Whilst this type of source has proved very effective at higher energies we note, as discussed elsewhere,³⁵ that at lower energies the thermal spread and space-charge effects limit the obtainable momentum resolution. The fact that the cathode is in close proximity to the target may also lead to surface contamination problems. The

authors designed their source with an aperture in the cathode to serve as an entrance slit for the spectrograph.

IV. SPIN POLARIZED INVERSE PHOTOEMISSION

We conclude our discussion of electron sources with a description of the electron source used in studies of spin polarized inverse photoemission (SPIPES). By using an incident electron beam that is spin polarized it is possible to examine the unoccupied exchange-split majority and minority bands above the Fermi level in ferromagnetic materials. This technique is the time-reversed analog of spin polarized photoemission.⁴⁰ However, SPIPES enjoys the advantage that, unlike spin polarized photoemission where the introduction of spin detection of the emitted photoelectrons leads to a drastic reduction in the real signal-to-noise level, the introduction of spin polarized electron beams leads to little or no reduction in the incident beam current and hence in the detected photon flux.

Spin polarized electron sources rely on the laser excitation of photoelectrons from the valence band into the conduction band of a gallium arsenide surface that has been exposed to cesium and oxygen. Exposure to these elements produces a surface with negative electron affinity, i.e., the conduction band lies just above the vacuum level. In the design due to Pierce *et al.*,⁴¹ circularly polarized light derived from a GaAsAl diode laser is used to excite direct transitions near the center of the Brillouin zone of a GaAs(001) surface. An alternative combination of laser and cathode used by Kirschner, Oepen, and Ibach⁴² is the He-Ne laser with a GaAs_{0.6}P_{0.4} cathode. Electrons excited into the conduction band are emitted from the cathode with their spin aligned either parallel ($s\uparrow$) or antiparallel ($s\downarrow$) to the axis of polarization of the incident laser beam. The spin polarization of the emitted electron beam is determined by the relative transition probabilities for the spin-orbit split valence bands. Thus, for a given circular polarization of the incident laser beam, this polarization P , defined by

$$P = \frac{s\uparrow - s\downarrow}{s\uparrow + s\downarrow}, \quad (15)$$

has a theoretical value of 50% for transitions from a $P_{3/2}$ state to a $S_{1/2}$ state. In practice, electron lifetimes and other cathode-related phenomena tend to reduce this polarization to typically 30%.⁴¹ The cathode is merely the source of electrons; a variety of lenses and 90° deflectors may follow in order to deliver the electrons to the target. Rather than presenting a detailed description of the properties of the electron beam obtained from such a source we refer the reader to the appropriate references, 41 and 42.

For IPES itself we note that the photocathode of these sources is potentially a high current electron source with the added advantage of higher-energy resolution (100 meV) than the unpolarized electron sources described above. It has been suggested that an electron beam with an energy spread of the order of 40 meV should be obtainable from a cooled photocathode.⁴³ However, this improvement in resolution is accompanied by a reduction in the beam current and as such, it is unlikely that it would prove to be the optimum source for "highest" resolution IPES.

An example of SPIPES is given in Fig. 13 where we

show the unoccupied majority and minority spin states above the Fermi level along the $\langle 110 \rangle$ direction of a Ni(110) crystal.⁴⁴ It will be seen that, as expected, only minority states exist above the Fermi level. The "spin resolved" spectra N_{\downarrow} and N_{\uparrow} plotted in Fig. 13 are obtained from the raw spectra n_{\downarrow} and n_{\uparrow} (photon counts with the incident spin aligned in opposite directions) through

$$N_{\uparrow} = \frac{n_{\uparrow} + n_{\downarrow}}{2} \left(1 + \frac{A}{\bar{P}} \right) \quad (16a)$$

and

$$N_{\downarrow} = \frac{n_{\uparrow} + n_{\downarrow}}{2} \left(1 - \frac{A}{\bar{P}} \right). \quad (16b)$$

A is the measured asymmetry $(n_{\uparrow} - n_{\downarrow}) / (n_{\uparrow} + n_{\downarrow})$ and \bar{P} is the projected component of the incident polarization P on the sample magnetization direction.

It is of interest to compare the counting statistics of the SPIPES experiment with the normal IPES experiment. If the incident electron beam were perfectly spin polarized, switching from one polarization to another would allow the sampling of a single spin state and the statistical error would be identical to the normal experiment, i.e., $1/\sqrt{n}$, where n is the count rate. However, with an incident beam of polarization P , both spin states are sampled and the statistical error in the spin measurement is increased to $1/\sqrt{P^2 n}$.⁴⁵ Thus, given equal incident currents, if P is typically 0.3,⁴¹ one has to increase the counting time of the spin measurement by a factor of 10 compared to the unpolarized measurement in order to achieve the same level of statistical accuracy. This efficiency factor of 10^{-1} should be compared with a factor of 10^{-4} characteristic of the spin detectors used in spin polarized photoemission.

V. CONCLUSIONS AND FUTURE PROSPECTS

In the previous sections we have reviewed the photon detectors and electron sources currently available for use in inverse photoemission. Clearly, the chosen combination of detector and source reflect the particular needs of the experiment. For experiments with low signal rates but with a requirement for reasonable resolution, isochromat detectors of the I_2/SrF_2 Geiger Muller type or the "solid state" equivalent are suitable, particularly when combined with large collection mirrors. With an electron source based on the BaO cathode, such an instrument provides an overall energy resolution of the order of 0.5 eV. For experiments on magnetic materials, the ability to measure the spin polarization of the unoccupied bands can only be achieved through the use of a spin polarized electron source. Combined with the Geiger Muller counter, it is again possible to achieve good resolution. Finally, if the detected photon energy is required to be tunable then the spectrograph is the instrument of choice. This instrument also offers the advantage of higher wavelength resolution.

This then represents the current state of the art in electron sources and photon detectors for IPES. The question remains as to how far the techniques can be pushed in the direction of higher resolution. In principle, it is possible to achieve extremely high resolution through the use of grat-

ings. For fixed entrance and exit armlengths, the resolving power of a grating spectrograph may be increased either by reducing the entrance slit width or by increasing the grating line density. In the absence of suitable electron optics, the former can be achieved by simply collecting photons at grazing emission. Unfortunately, both modifications lead to a reduction in the measured signal. One can compensate for such a reduction by increasing the incident electron flux but only within the limits defined by space-charge effects. The space-charge limitation, which is greater at low electron energies, contrasts directly with optimization of the resolving power of a grating, which is easiest at low photon energies. With some compromise it is clearly possible to achieve the required photon wavelength resolution. The major problem limiting improvement in overall resolution is the identification of an electron source with energy spread less than 0.1 eV and sufficient flux to allow a reasonable signal rate. We suggest that this provides the immediate challenge for the advancement of the IPES technique.

ACKNOWLEDGMENTS

We are pleased to acknowledge valuable interactions with R. F. Garrett, M. R. Howells, G. C. Smith, N. V. Smith, and N. G. Stoffel. This work was supported by the Division of Materials Sciences, U.S. Department of Energy, under Contract No. DE-AC02-76CH00016.

- ¹ V. Dose, *Prog. Surf. Sci.* **13**, 25 (1983); N. V. Smith, *Rep. Prog. Phys.* **51**, 1227 (1988).
- ² E. W. Plummer and W. Eberhardt, *Adv. Chem. Phys.* **49**, 533 (1982).
- ³ J. B. Pendry, *J. Phys. C* **14**, 1381 (1981).
- ⁴ P. D. Johnson and J. W. Davenport, *Phys. Rev. B* **31**, 7521 (1985).
- ⁵ R. L. Park and J. E. Houston, *Phys. Rev. B* **6**, 1073 (1972).
- ⁶ J. Stohr and R. Jaeger, *Phys. Rev. B* **26**, 4111 (1982).
- ⁷ K. Giesen, F. Hage, F. J. Himpsel, J. H. Reiss, and W. Steinmann, *Phys. Rev. Lett.* **55**, 300 (1985).
- ⁸ N. V. Smith, C. T. Chen, J. M. Tranquada, and P. D. Johnson, *Phys. Rev. B* **38**, 12259 (1988).
- ⁹ J. K. Lang and Y. Baer, *Rev. Sci. Instrum.* **50**, 221 (1979).
- ¹⁰ G. Denninger, V. Dose, and M. Scheidt, *Appl. Phys.* **81**, 375 (1979).
- ¹¹ J. A. R. Samson, *Techniques of Vacuum Ultraviolet Spectroscopy* (Wiley, New York, 1967).
- ¹² V. Dose, Th. Fauster, and R. Schneider, *Appl. Phys. A* **40**, 203 (1986).
- ¹³ P. M. G. Allen, P. J. Dobson, and R. G. Egdell, *Solid State Commun.* **55**, 701 (1985).
- ¹⁴ D. Funnemann and H. Merz, *J. Vac. Sci. Technol. A* **5**, 657 (1987).
- ¹⁵ K. Desinger, V. Dose, M. Glöbl, and H. Scheidt, *Solid State Commun.* **49**, 479 (1984); see also R. A. Bartynski and T. Gustafsson, *Phys. Rev. B* **33**, 6588 (1986).
- ¹⁶ W. R. Hunter, *Opt. Acta* **9**, 255 (1962).
- ¹⁷ N. Babbe, W. Drube, I. Schäfer, and M. Skibowski, *J. Phys. E* **18**, 158 (1985).
- ¹⁸ I. Schäfer, W. Drube, M. Schluter, A. Plagemann, and M. Skibowski, *Rev. Sci. Instrum.* **58**, 710 (1987).
- ¹⁹ G. Chauvet and R. Baptist, *J. Electron. Spectrosc.* **24**, 255 (1981).
- ²⁰ G. Chauvet, A. Brenac, and R. Baptist, *Rev. Sci. Instrum.* **58**, 197 (1987).
- ²¹ P. D. Johnson, S. L. Hulbert, R. F. Garrett, and M. R. Howells, *Rev. Sci. Instrum.* **57**, 1324 (1986).
- ²² Th. Fauster, F. J. Himpsel, J. J. Donelon, and A. Marx, *Rev. Sci. Instrum.* **54**, 68 (1983).
- ²³ Th. Fauster, D. Straub, J. J. Donelon, D. Grimm, A. Marx, and F. J. Himpsel, *Rev. Sci. Instrum.* **56**, 1212 (1985); P. T. Andrews, *Vacuum* **38**, 257 (1988).
- ²⁴ P. D. Johnson and N. V. Smith, *Phys. Rev. B* **27**, 2527 (1983).
- ²⁵ P. M. Echenique, F. Flores, and F. Sols, *Phys. Rev. Lett.* **55**, 2348 (1985).

- ²⁶ P. D. Johnson, X. Pan, J. Tranquada, S. L. Hulbert, and E. Johnson, *DIET III*, edited by R. H. Stulen and M. L. Knotek (Springer, Berlin, 1988), p. 73.
- ²⁷ P. Laporte and J. L. Subtil, *J. Opt. Soc. Am.* **72**, 1558 (1982).
- ²⁸ T. T. Childs, W. A. Royer, and N. V. Smith, *Rev. Sci. Instrum.* **55**, 1613 (1984).
- ²⁹ S. L. Hulbert, P. D. Johnson, N. G. Stoffel, W. A. Royer, and N. V. Smith, *Phys. Rev. B* **31**, 6815 (1985).
- ³⁰ W. Altmann, K. Desinger, M. Donath, V. Dose, A. Goldmann, and H. Scheidt, *Surf. Sci.* **151**, L185 (1985).
- ³¹ K. H. Frank, H. -J. Sagner, E. E. Koch, and W. Eberhardt, *Phys. Rev. B* **38**, 8501 (1988).
- ³² W. A. Royer and N. V. Smith, *Rev. Sci. Instrum.* **59**, 737 (1988).
- ³³ V. Dose, H. -J. Gossmann, and D. Staub, *Phys. Rev. Lett.* **47**, 608 (1981).
- ³⁴ D. P. Woodruff and N. V. Smith, *Phys. Rev. Lett.* **48**, 283 (1982).
- ³⁵ N. G. Stoffel and P. D. Johnson, *Nucl. Instrum. Methods A* **234**, 230 (1984).
- ³⁶ J. R. Pierce, *Theory and Design of Electron Beams* (Van Nostrand, New York, 1954), Chap. 9.
- ³⁷ B. Reihl and K. H. Frank, *Phys. Rev. B* **31**, 828 (1985); K. H. Frank, R. Dudde, H. -J. Sagner, and W. Eberhardt, *Phys. Rev. B* **39**, 940 (1989).
- ³⁸ P. W. Erdman and E. C. Zipf, *Rev. Sci. Instrum.* **54**, 62 (1982).
- ³⁹ A. Brenac, Thesis, Université Scientifique Technologique et Médicale de Grenoble (1987).
- ⁴⁰ R. Feder, Ed., *Polarized Electrons in Surface Physics* (World Scientific, Singapore, 1985).
- ⁴¹ D. T. Pierce, R. J. Celotta, G. C. Wang, W. N. Unertl, A. Galejs, C. E. Kuyatt, and S. R. Mielczarek, *Rev. Sci. Instrum.* **51**, 478 (1980).
- ⁴² J. Kirschner, H. P. Oepen, and H. Ibach, *Appl. Phys. A* **30**, 177 (1983).
- ⁴³ C. S. Feigerle, D. T. Pierce, A. Seiler, and R. J. Celotta, *Appl. Phys. Lett.* **44**, 866 (1984).
- ⁴⁴ J. Unguris, A. Seiler, R. J. Celotta, D. T. Pierce, P. D. Johnson, and N. V. Smith, *Phys. Rev. Lett.* **49**, 1047 (1982).
- ⁴⁵ J. Kessler, *Polarized Electrons* (Springer, Berlin, 1976).

PRICING AND ORDERING INFORMATION FOR REVIEW-ARTICLE REPRINTS

PRICES: \$5.00; \$4.50 each for bulk orders of ten or more copies of the same article sent to one address. Delivery is via surface mail. Airmail delivery available at the following surcharge: \$2.50 for the first copy plus \$1.00 for each additional copy sent to one address. *Reprint orders must be prepaid.*

ORDERS: Please specify REVIEW OF SCIENTIFIC INSTRUMENTS REVIEWS and give the article title, authors, month, and year of publication, and the page number of the article's title page. Send orders accompanied by payment in full (make checks payable to American Institute of Physics) to: *Current Physics Reprints, American Institute of Physics, 335 East 45th Street, New York, NY 10017.*
